Cancer Nanotechnology

RESEARCH Open Access

Effective combination of biocompatible zinc oxide nanocrystals and high-energy shock waves for the treatment of colorectal cancer

Luisa Racca[1†], Giada Rosso[1†], Marco Carofiglio[1], Sharmila Fagoonee[2,3], Giulia Mesiano[1], Fiorella Altruda[2,3] and Valentina Cauda[1*]

[†]Luisa Racca and Giada Rosso have contributed equally to this work

*Correspondence: valentina.cauda@polito.it

[1] Department of Applied Science and Technology, Politecnico di Torino, C.So Duca Degli Abruzzi 24, 10129 Turin, Italy
[2] Institute of Biostructure and Bioimaging, National Research Council (CNR), Via Nizza 52, 10126 Turin, Italy
[3] Molecular Biotechnology Center Guido Tarone, University of Turin, Via Nizza 52, 10126 Turin, Italy

Abstract

Background: Colorectal cancer (CRC) is the third most diagnosed tumor worldwide, with a very high mortality rate, second only to lung cancer. Current treatments, such as surgery, chemotherapy or radiotherapy, are not effective enough and show several limitations. Among the emerging strategies, nanomedicine offers very powerful tools in cancer treatment. Recently, the combination of nanoparticle antitumor effect with a triggering external stimulation was formulated to boost up the cytotoxic activity.

Results: In this work, we show the synergistic effect of oleic acid-capped zinc oxide nanocrystals (ZnO NCs) and mechanical high-energy shock waves (SW) in the treatment for CRC cells, in vitro. We tested two different types of ZnO NCs synthetized in our laboratory, the basal undoped ZnO NCs and the iron-doped ones (Fe:ZnO NCs). The presence of the oleic acid capping and the further amino-propyl functionalization guarantee a high colloidal stability to both NCs, while the iron doping confers to Fe:ZnO NCs interesting magnetic properties useful for imaging applications in a clinical perspective. Thus, the iron-doped ZnO NCs are very attractive as potentially theranostic nanoparticles, allowing both stimuli-responsive therapy and magnetic resonance imaging.

Importantly, two colon adenocarcinoma cell lines, the HT-29 and the Dukes' type C Colo 320DM cells were tested, both showing a good bio-tolerance and internalization rates of NCs. With the aim of eradicating the CRC cells, the possible synergism between the undoped/iron-doped ZnO NCs and an external physical stimulus, i.e., high-energy SW, was then here investigated in vitro. We demonstrated that the combined treatment resulted in an augmentation of the antitumor activity, especially for Colo 320DM cells, when compared to controls. Moreover, a repeated and sequenced SW treatment (three times/day, 3SW) after ZnO NCs exposure resulted in a further increased mortality of CRC cells.

Conclusion: Our work proposes the combination of the cytotoxic activity of ZnO NCs with the SW external stimulation to obtain a booster of the antitumor activity, which warrants further investigation in vivo on CRC as well as on other tumors.

Keywords: Nanoparticle-assisted shock waves, Stimuli-responsive therapy, Colorectal cancer, Cell death mechanisms, Iron-doped ZnO nanoparticles

Graphical Abstract

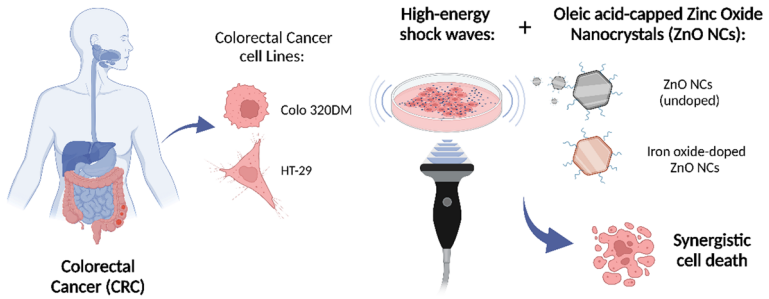

Background

Colorectal cancer (CRC) is the third most diagnosed cancer and the second for mortality after lung cancer (Sung et al. 2021), but its cases are rapidly growing (Sawicki et al. 2021). Surgical removal, chemotherapy and radiotherapy are the first-line treatments for this disease, even if it is frequently reported how their use is associated with the development of severe side effects and is subjected to other important limitations, as the occurrence of resistances. For these reasons, novel strategies, e.g., targeted therapies with monoclonal antibodies or nanomedicine, are emerging as alternative candidates for the treatment of CRC (Xie et al. 2020; Pavitra et al. 2021). Nanomedicine, the branch of medicine that develops and studies nanosized materials (smaller than 100 nm) for therapeutic and diagnostic applications, particularly contributes to the expansion of new strategies to identify and treat CRC in different ways (Brar et al. 2021; Cisterna et al. 2016).

A first possibility is to exploit nano-objects, e.g., liposomes or nanoparticles, for the delivery of therapeutic agents to the target site, avoiding the poor selectivity and solubility of several anticancer drugs. These nanotools could even be equipped with tumor-associated ligands to specifically target cancer cells, further increasing the selectivity and thus the therapeutic outcomes. Therefore, some nanoplatforms composed by nanoparticles for drug delivery are nowadays under clinical trial for colorectal cancer (Pavitra et al. 2021; Brar et al. 2021; Cisterna et al. 2016).

Secondly, nanoparticles can act themselves as toxic agents. In this case, a promising candidate is represented by zinc oxide nanoparticles (ZnO NPs) that possess an intrinsic selective cytotoxicity toward cancer cells (Carofiglio et al. 2021; Racca et al. 2018). Actually, zinc is an essential element for life, and its imbalance could be detrimental (Skrajnowska and Bobrowska-Korczak 2019). ZnO NPs could thus directly provoke severe damages due to their dissolution and consequent release of zinc ions, and because of their capability to generate reactive oxygen species (ROS) (Racca et al. 2018). There are several examples in the literature of the application of ZnO NPs for the treatment of colorectal cancer, evidencing their relevant cytotoxicity (Jiang et al. 2018), even when compared with other nanomaterials, as silver (Song et al. 2014) and aluminum oxide (Subramaniam et al. 2019). ZnO NPs, however, have some drawbacks that limit their application, principally due to their uncontrolled degradation (Garino et al. 2019). A possible approach to solve this limit is to shield the nanoparticles, e.g., with polymers,

capping agents, graphene oxide or phospholipids (Dumontel et al. 2017; Dumontel et al. 2019; Laurenti et al. 2019; Ancona et al. 2018), or through the insertion of new chemical species inside their structure, i.e., by doping the nanoparticles (Carofiglio et al. 2020; Bharat et al. 2019; Barui et al. 2020). The latter approach in particular preserves, and in some cases, improves the ZnO properties, better enhancing the stability against premature dissolution. Iron doping has been extensively explored because it confers magnetic properties to ZnO NPs, useful for magnetic resonance imaging, and improves the metal oxide stability and biocompatibility, limiting its dissolution into Zn^{2+} cations (Carofiglio et al. 2021; Carofiglio et al. 2020; Xia et al. 2011).

In the last years, many researchers focused on the use of nanoparticles that can operate in synergy with other agents, i.e., external physical stimulations such as light, magnetic fields or mechanical pressure waves, to cause cancer cell death. This combined intervention aims to confine the toxic outcomes only when the two components are administered together into the tumor, to prevent the development of side effects and maximize the efficacy (Racca and Cauda 2021). In some cases, the nanoparticles do not really possess an active role in the process, e.g., when they only deliver the agent that synergistically works with the physical input (Nompumelelo Simelane et al. 2020). In the case of colorectal cancer, there are some examples of nanoparticles carrying photosensitive drugs, such as cisplatin (Pavitra et al. 2021), porphyrins and others (Nompumelelo Simelane et al. 2020), which are triggerable by an external physical stimulation, as light for photothermal or photodynamic therapy, and thus able to deplete cancer cells. Differently, in other investigations the nanoparticles' role is crucial because they actively interact with the stimulation to trigger cell death, avoiding the necessity to incorporate other compounds. Several nanomaterials like gold (Cabeza et al. 2020; Goodrich et al. 2010), titanium oxide (Zhang and Sun 2004), zinc oxide (Ancona et al. 2018) and iron oxide (Palzer et al. 2021) nanoparticles have been proposed for this purpose, typically in combination with light or magnetic inputs (Racca and Cauda 2021). The use of mechanical pressure waves, i.e., ultrasound (US) and shock waves (SW), is particularly intriguing due to their current use in clinical practice, low-cost of instrumentation, their focusing capability, and their great penetration depth in tissues (Racca and Cauda 2021; Canavese et al. 2018). Additionally, mechanical pressure waves can induce both thermal and non-thermal effects, leading to thermoablation or to acoustic cavitation, respectively. The combination of mechanical pressure waves with drugs and nanoparticles can maximize the efficacy of the therapeutic outcomes, even if the mechanism of this synergism is often multifaceted and challenging to elucidate (Racca and Cauda 2021; Canavese et al. 2018). It has been indeed reported that several harmful conditions, related to thermal, mechanical or chemical damages could take place (Racca and Cauda 2021). In this perspective, the SW treatment is particularly attractive because it is associated by a reduced increment of the temperature in comparison with the ultrasound one, while it involves the activation of molecules and nanoparticles to exploit a therapeutic action, similarly to US (Racca et al. 2020; Wan et al. 2016). In the literature there are some examples of nanoparticles working synergistically with a mechanical pressure wave input, mainly involving gold nanoparticles (Beik et al. 2018; Sazgarnia et al. 2013), metal organic frameworks (Zhong et al. 2022; Liang et al. 2021), titanium oxide (Matos et al. 2020; Vighetto et al. 2021) and zinc oxide (Racca et al. 2020; Vighetto et al. 2019). An example is represented

by the investigation of Sazgarnia et al., where gold nanoparticles were employed in combination with US or with both US and light for the depletion of colon cancer in vitro and in vivo. It was highlighted that nanoparticles and US were able to trigger cell death, even if the maximum effect was achieved with the addition of light (Sazgarnia et al. 2013).

Differently from the previous literature, in the present work we propose the use of oleic acid capped, amino-propyl functionalized zinc oxide nanocrystals (ZnO NCs), undoped or doped with iron, as effective therapeutic agents in combination with SW for the efficient killing of two CRC cell lines, the colon adenocarcinoma HT-29 and Dukes' type C Colo 320DM, as depicted in Fig. 1. The chemical and biological features of pristine ZnO NCs were compared with the iron-doped ones. The surface functionalization confers to both nanocrystals a high colloidal stability and good biocompatibility. Furthermore, the Fe-doped ZnO NCs are particularly intriguing for further in vivo investigations because of the magnetic properties conferred by the iron doping that allows their use for magnetic resonance imaging purposes. In this sense, these NCs could in future act both as therapeutic and diagnostic nanotools, becoming theranostic nanoparticles, very attractive for potential clinical translations (Carofiglio et al. 2021). We thus propose here the evaluation of both NC types with shock wave stimulation for the treatment of colorectal cancer cells, aiming at the efficient depletion of colon cancer in vitro and to pave the way for future in vivo treatments.

Materials and methods

NCs synthesis and characterization

Undoped (ZnO NCs) and 6 at.% iron-doped (Fe:ZnO NCs) NCs were synthetized following a procedure already exploited in previous works (Carofiglio et al. 2021). Briefly, 526 mg of zinc acetate dihydrate (Sigma-Aldrich) was dissolved in 40 ml of ethanol (99%, Sigma-Aldrich). For doped NCs, 58 mg of ferric nitrate nonahydrate

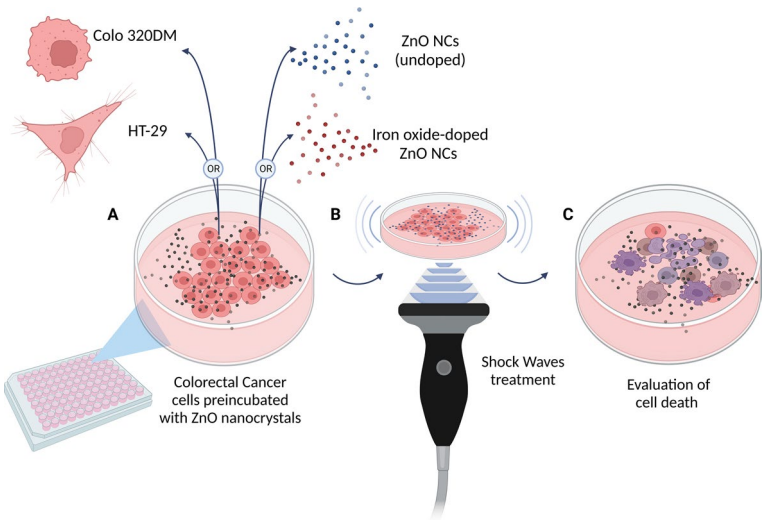

Fig. 1 Scheme of the combined action of zinc oxide nanocrystals (ZnO NCs) and shock waves (SW) treatments proposed in this study on two colon adenocarcinoma cell lines: Dukes' type C Colo 320DM and HT-29. **A** Cells were preincubated with undoped ZnO NCs or, alternatively, with iron-doped ZnO NCs. Successively, **B** cells underwent the SW treatment and finally **C** cell death was evaluated. Created with BioRender.com

(Sigma-Aldrich) was also added to the ethanolic solution as precursor for iron doping. The dissolved salts were placed in a round bottom flask under moderate stirring and 1 ml of bidistilled water coming from a Direct Q3 system (Millipore) was also included in the solution. Finally, 140 µl of oleic acid (Sigma-Aldrich) was added and the solution heated up to 70 °C in refluxing conditions. When the target temperature was reached, a solution of tetramethylammonium hydroxide (TMAH, Sigma-Aldrich) containing 1.044 g of TMAH, 10 ml of water and 1.052 ml of bidistilled water was rapidly poured into the flask to allow nanoparticles formation. The nanoparticles suspension was collected after 10 min and cooled down by adding 40 ml of ethanol at 0 °C. Three times of centrifugation and redispersion steps were exploited to wash the NCs from unreacted moieties.

NCs were also functionalized with amino propyl groups, following a standard protocol that was already used in other works for ZnO nanoparticles (Garino et al. 2019; Dumontel et al. 2017; Vighetto et al. 2022). More in detail, the nanoparticles were suspended in ethanol at the concentration of 2.5 mg/ml, heated in a round bottom flask at 70 °C and stripped with nitrogen. 10%mol of 3-aminopropyltrimethoxysilane (APTMS, Sigma-Aldrich) with respect to the ZnO NCs was included. The reaction ran for 6 h and then NCs were centrifuged and resuspended three times.

The crystallinity of the NCs was checked with X-ray diffraction analysis. NCs were deposited onto a pure silicon wafer and analyzed with a Panalytical X'Pert diffractometer. Similarly prepared samples were used for morphological and elemental analysis with field emission scanning electron microscopy (FESEM). A SUPRA 40 (Zeiss) with an energy dispersive X-ray spectroscopy detector (EDS, by Inca Oxford) was exploited to perform the measurements on both undoped and Fe-doped NCs. For high-resolution transmission electron microscopy (HR-TEM) measurements, 10 µl of 50 µg/ml NCs suspensions in water was deposited onto a Lacey Carbon Support Film (300 mesh, Cu, Ted Pella Inc.) and analyzed with a Talon™ F200X G2 S(TEM) from Thermo Scientific at an operating voltage of 200 kV. Finally, dynamic light scattering (DLS) and Z-potential analyses were performed on 100 µg/ml of colloidal suspension in ethanol and water with a Zetasizer Nano ZS90 (Malvern Panalytical).

Cell lines

Human colorectal adenocarcinoma cell lines HT-29 (HTB-38® from ATCC) and Colo 320DM (CCL-220® from ATCC) were both grown in 25 or 75 cm^2 treated flasks (Corning) with RPMI 1640 (ATCC) supplemented with 10% heat inactivated fetal bovine serum (ATCC) and 1% penicillin streptomycin solution (Sigma-Aldrich), as previously described (Manco et al. 2021; Fuentes-Vélez 2021). All cells were maintained in a humidified incubator at 37 °C with an atmosphere of 5% CO_2. Cells were periodically tested for mycoplasma infection.

While HT-29 colorectal cancer cells grow adherent to the flask and form dense cell colonies, Colo 320DM cells are weakly attached to the flask and grow both in adhesion and suspension (Tommelein et al. 2016). They were indeed isolated from a Dukes' type C colon carcinoma, characterized by invasion through the bowel wall (Haq et al. 2009).

Analysis of NC-induced cytotoxicity

NCs solutions were always freshly prepared prior to performing the assays. The NCs stock solution in ethanol was sonicated for 10 min, then the NCs were diluted into complete culture medium to obtain the desired treatment dispersions.

NCs cytotoxicity in colorectal cancer cells was evaluated with the WST-1 assay (Roche) at two time points (24 or 48 h). Briefly, both cell lines were plated (5′000 cells/well in 100 µl) with the treatment solutions (0–5–10–15–20 µg/ml) in replicates in treated 96-well plates (Greiner Bio-One). In proximity of the desired time points (24 or 48 h incubation) 10 µl of the WST-1 solution/well was added, and after 2 h (HT-29) or 4 h (Colo 320DM) cell viability was estimated measuring absorbance at 450 nm with the Multiskan GO microplate spectrophotometer (Thermo Fisher Scientific) with a reference wavelength of 620 nm. The background absorbance, i.e., the value obtained by the sample without cells, was subtracted to all the absorbance values obtained. The background-subtracted absorbance of the untreated cells was set as 100% viability, with all the others results as percentage of cell viability relative to untreated cells. Experiments were run in multiple replicates, with $n \geq 3$ and errors expressed as SEM (standard error mean).

Quantification of cellular uptake of NCs

NCs were labeled with Atto647-NHS ester dye (Thermo Fisher Scientific) at a ratio of 2 µg of dye per mg of NCs, followed by preparation of treatment solutions as described above.

In this case, 250′000 cells were plated into treated 6-well plate (Corning) with 2.5 ml of the treatment solutions (0–5–10 µg/ml). After 5, 24 and 48 h of incubation at 37 °C and 5% CO_2, cells were washed with PBS, trypsinized, and analyzed with flow cytometer Guava Easycyte 6–2L (Merck Millipore), comparing the curve of untreated cells with the curves obtained by cells incubated with fluorescently labeled NCs in terms of percentage of positive events, evaluating the percentage of the cell population with a fluorescence intensity over the curve obtained from untreated cells. Representative histograms were obtained with the software FCS Express (DeNovo Software).

Treatment with mechanical pressure waves

The possible synergy between NCs and SW was evaluated in both cell lines, plating 5′000 cells/100 µl with or without NCs (10 µg/ml) in treated 96-well plates (Greiner Bio-One). After 24 h incubation, plates were exposed to PW^2 instrument (Richard Wolf device, ELvation Medical GmbH) for the treatment with SW (0.12 mJ/mm^2, 250 shots, 4 shots/s). In particular, a small amount of ultrasound coupling gel was placed on the top of the SW probe to avoid possible loss of signal due to the presence of air and the plate was directly put on the top of the probe. After 24, 48 or 72 h from the treatment, cell proliferation was measured with the WST-1 assay.

After a first exploration, where a single SW treatment was administered, the effects of three consecutive treatments were evaluated (3SW). In this case, the same protocol was employed, but after 24 h incubation with NCs, cells were exposed to 3SW treatment (each of 0.12 mJ/mm^2, 250 shots, 4 shots/s) in a day, i.e., a treatment every 4 h. 24, 48 or

72 h after the last SW treatment, cell proliferation was estimated using the WST-1 assay. In all the presented treatments, also control assays were performed: untreated cells, cells treated with NCs only, cells tested with SW or 3SW only.

Evaluation of cell membrane integrity

A cell membrane integrity assay was carried out during and after the 3SW on both HT-29 and Colo 320DM cells incubated with Fe:ZnO NCs or ZnO NCs. In details, both cell lines were incubated with 10 μg/ml of NCs in 96-well plates. After 24 h of NCs incubation, cells were then exposed to 250 shots of SW (0,12 mJ/mm^2 4 shots/s) for three times (a treatment every 4 h). Control cell groups remained untreated, or were treated with ZnO or Fe:ZnO NCs or with 3SW only. Immediately after each single SW treatment, as well as 24, 48 and 72 h after the last SW treatment, the cell culture medium was replaced with a solution of 1.5 μM propidium iodide (PI, as indicator of membrane integrity) in PBS (Marino et al. 2019). Cells were then observed under a wide-field fluorescence-inverted microscope (Eclipse Ti-E, Nikon).

ROS generation analysis under shock wave stimulation

The ZnO and Fe:ZnO NCs were investigated in terms of reactive oxygen species (ROS) production under shock wave stimulation using Electron Paramagnetic Resonance (EPR) spectroscopy coupled with the spin-trapping technique. More in detail, 1.5 μg of NCs was withdrawn from the ethanolic stock solution and firstly dispersed in 90 μl of bidistilled water. The solution was placed in a 96-well plate for cell culture (TC-Treated, Corning). Then 10 μl of a water solution of a spin trap (5,5-dimethyl-L-pyrroline-N-Oxide, DMPO, Sigma-Aldrich) at a concentration of 100 mM was added to the dispersion. The final concentration of NCs was 15 μg/ml while the DMPO final concentration for each sample was 10 mM. The Fe:ZnO or ZnO NCs containing well was stimulated from the bottom with a high-energy focalized shock wave (SW) device PW^2 (R. Wolf, ELvation Medical) with the same conditions exploited for cells treatment. The well and the transducer were acoustically coupled with a gel (Stosswellen Gel, ELvation Medical GmbH). After the stimulation, a small volume of the NPs dispersion was withdrawn by means of a quartz capillary and analyzed with an EMXNano X-Band spectrometer (Bruker, center field 3426 G, 10 scans, 60 s sweep time). The spectra were processed with Bruker Xenon software (Bruker).

Cell death assay

Since the synergistic effects were particularly increased in Colo 320DM cells even after one SW treatment, the investigation of cell death kinetic was performed only in this cell line. Colo 320DM cells were plated (5′000 cells/100 μl culture medium with or without NCs) in a black 96-well plate with clear bottom (Corning). The kinetic evaluation of cell apoptosis and necrosis was performed with the RealTime-Glo Annexin V Apoptosis and Necrosis Assay (Promega). 24 h after cell plating, 100 μl of the reaction mix containing all the substrate for the reaction was added to each well and the luminescence and the fluorescence (485 ± 20 nm excitation range, 525 ± 30 nm emission range) signals were collected by the microplate reader Glomax (Promega). Cells were then divided in treatment groups: SW, ZnO NCs + SW and Fe:ZnO NCs + SW and were then treated with

SW. Measurements were performed immediately after SW treatment (0 min) and after 30 min, 1 h, 2 h, 4 h, 6 h and 24 h.

Statistical analyses

All experiments were performed at least three times. Data were always shown as mean ± standard error mean (SEM). Two- and three-ways analysis of variance (ANOVA) statistical tests were used to assess statistical significance, with a $p < 0.05$ being considered significant. All analyses and graphs were obtained by with Origin (OriginLab).

Results

Synthesis and characterization of NCs

Doped and undoped NCs, both with oleic acid capping and amino-propyl functionalization, were first thoroughly characterized from the morphological, structural and colloidal stability points of view.

As depicted in Fig. 2A, the X-ray diffraction (XRD) patterns of both NCs showed the same diffraction peaks which can be attributed to the wurtzitic crystalline structure of ZnO (JCPDS-ICDD, card No. 89-1397). No peaks indicating the metallic iron or iron oxide phases were found, suggesting the absence of additional Fe-related crystalline phases (Carofiglio et al. 2021). The Debye–Scherrer formula (Patterson 1939) applied to the (100) diffraction peak allows to calculate an average crystallite dimension of 10 nm and 11 nm, for Fe:ZnO and ZnO NCs, respectively. Moreover, the FESEM images (Fig. 2C) indicated that both NCs have an almost spherical shape with a diameter between 4 and 10 nm. The elemental analysis performed through EDS demonstrated the inclusion of iron inside the nanoparticles. Indeed, a ratio between Fe atoms and Zn atoms of 0.057 was found, in agreement with the amount exploited during the synthesis. High-resolution TEM images (Fig. 2D) show tiny single-crystals, almost spherical in shape. No differences can be appreciated between the Fe-doped and the undoped NCs. These data confirm a previous study on iron-doped nanoparticles by some of us (Carofiglio et al. 2021). In that work, we reported that iron assumes both the Fe^{+2} and Fe^{+3} states, with a slight preponderance of Fe^{3+} oxidation state for the NCs doped with a 6 at% of iron with respect to zinc. Moreover, the inclusion of iron inside the NCs crystalline structure induce novel magnetic responsiveness with respect to the pure ZnO NCs counterparts (as reported in Additional file 1: Figure S1) in terms of maximum magnetization, with consequent potentialities in magnetic resonance imaging (MRI).

DLS and Z-potential analyses (Fig. 2B) demonstrated the high stability of ZnO NCs in both ethanol and water, without evidencing differences between undoped and doped NCs. More in detail, the hydrodynamic diameter of ZnO NCs in ethanol was measured to be 51 nm with a polydispersity index (PDI) of 0.137, while Fe:ZnO NCs showed a hydrodynamic diameter of 92 nm and a PDI of 0.168. In water, the hydrodynamic diameter is slightly larger, with values of 70 nm and 104 nm for undoped and Fe-doped ZnO NCs, respectively, with 0.142 and 0.162 of PDI, indicating a very low increase of aggregation degree when the medium is changed and a still high level of monodispersion. The Z-potential was also measured in water with + 22.3 mV and + 25.9 mV for ZnO and Fe:ZnO NCs, respectively. These high positive values agree with the monodispersed size distributions, showing that both types of NCs are stable colloidal suspensions.

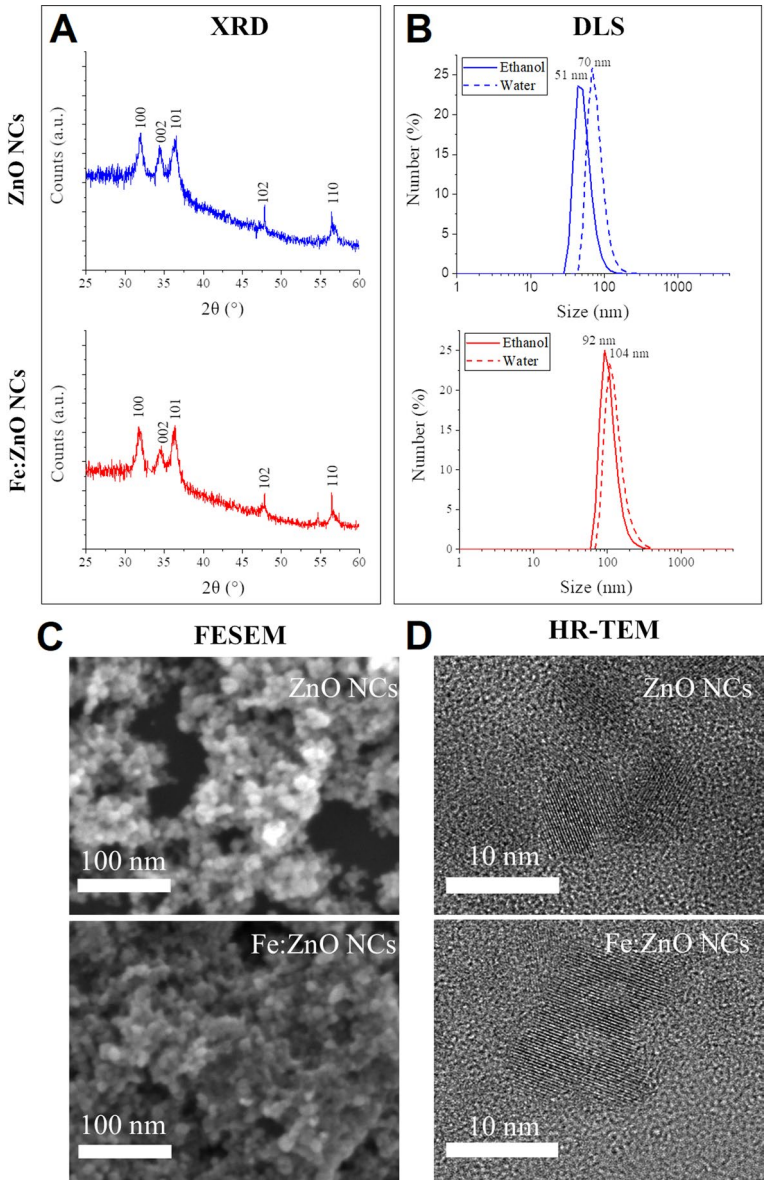

Fig. 2 Characterization of oleic acid capped, amino-propyl functionalized undoped (ZnO NCs) and doped (Fe:ZnO NCs) NCs. **A** X-ray diffraction (XRD) spectra of ZnO NCs and Fe:ZnO NCs. **B** Dynamic light scattering (DLS) in ethanol and water analysis of ZnO NCs and Fe:ZnO NCs. **C** Field-emission scanning electron microscopy (FESEM) images of ZnO NCs and Fe:ZnO NCs. **D** High-resolution transmission microscopy (HR-TEM) images of ZnO NCs and Fe:ZnO NCs

Treatment with NCs induces cytotoxicity in CRC cells

The cytotoxic effect of both Fe:ZnO and ZnO NCs was assessed on HT-29 and Colo 320DM cell lines after 24 and 48 h of NCs exposure. As depicted in Fig. 3, doped and undoped NCs displayed a dose-dependent antitumor effect in CRC cells, with an increased mortality at higher concentrations of NCs. Interestingly, different toxicity profiles between the two cell lines were observed.

Concerning HT-29 cells (Fig. 3A), no differences in cell viability were reported between doped and undoped ZnO NCs exposure up to 10 μg/ml (after both 24 and 48 h). Instead,

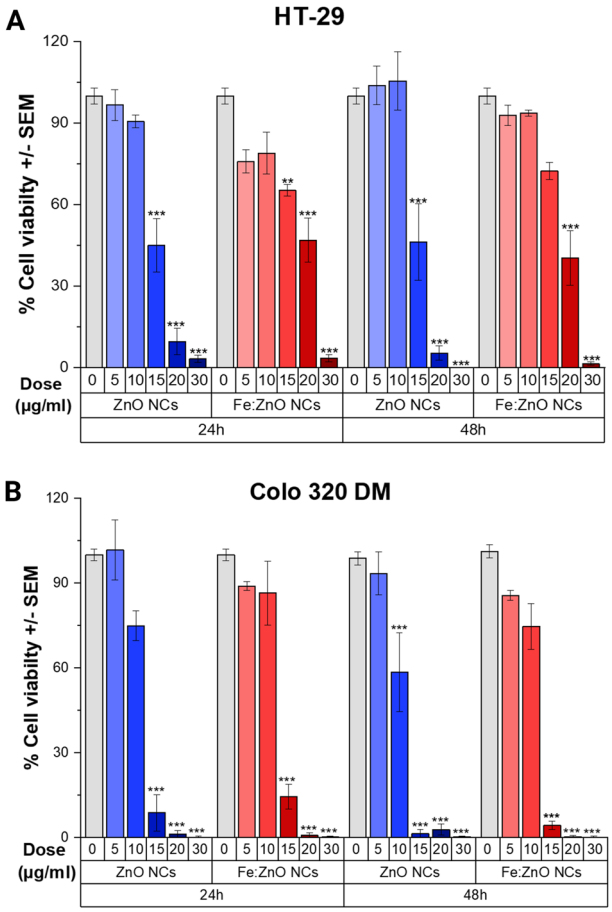

Fig. 3 Cytotoxicity of ZnO NCs and Fe:ZnO NCs on HT-29 (**A**) and Colo 320DM (**B**) at different concentrations (0–5–10–15–20–30 µg/ml) and time points (24 and 48 h) measured with the WST-1 assay. Data are expressed as percentage of cell viability mean ± SEM. n ≥ 3. Statistical relevance is indicated in comparison with control sample (* $p < 0.05$, ** $p < 0.01$, *** $p < 0.001$)

at the concentration of 15 µg/ml of ZnO NCs and Fe:ZnO NCs, after a 24-h exposure, the cell viability dropped down to 45 ± 10% and to 65 ± 2%, respectively. The same trend was repeated after 48 h exposure to 15 µg/ml of undoped and doped NCs with a mean cell viability of 46 ± 14% with ZnO NCs and 72 ± 3% with Fe:ZnO NCs. At 20 µg/ml the cell viability resulted less than 10% with ZnO NCs at both time points (9 ± 5% at 24 h, 5 ± 3% at 48 h), while a residual viability of ≥ 40% was still assessed with Fe:ZnO NCs (47 ± 8% at 24 h, 40 ± 10% at 48 h). These data suggest a higher biocompatibility of the iron-doped ZnO NCs towards the tested cancer cells than the undoped NC. Interestingly, as already observed in a previous study on KB cervical adenocarcinoma cell line (Racca et al. 2020), a slight increase of HT-29 cell viability was observed with the lowest dosages (5–10 µg/ml) after 48 h incubation, probably due to the role of Zn^{2+} ions activating ERK and Akt signaling pathways (Liu et al. 2017).

The viability of Colo 320DM (Fig. 3B) was significantly affected by both NC types at concentrations higher than 15 µg/ml, while cell viability was ≥ 60% for both 5 and 10 µg/ml concentrations. Even in this case, a slightly lesser toxicity was shown by the iron-doped NCs. Furthermore, the cell viability of Colo 320DM was affected by the NCs more

extensively than in HT-29 cells, thus the slight increase in cell proliferations was evident only for the 5 μg/ml dosage after 24 h incubation.

CRC cells successfully internalize NCs

The percentage of cells internalizing fluorescently labeled ZnO NCs was estimated through a dedicated flow cytometry assay. In this experiment, both 5 and 10 μg/ml concentrations of NCs were used as they showed the highest cytocompatibility. After the exposure, cells displaying an increased fluorescence than the untreated controls were assessed as cells internalizing ZnO NCs or at least with NCs adherent to their surface, as representatively reported in Additional file 1: Figure S2. In Fig. 4 the percentage of positive events gradually increased in both cell lines at higher NCs concentrations and incubation times, reaching an optimum at 10 μg/ml and 24 h incubation, with a percentage of positive events of 89 ± 1% with ZnO NCs and 92 ± 2% with Fe:ZnO NCs for HT-29 (Fig. 4A), and 82 ± 10% with ZnO NCs and 71 ± 3% with Fe:ZnO NCs for Colo 320DM (Fig. 4B). These conditions were thus chosen for further investigations with SW.

Synergistic treatment with shock waves and NCs remarkably decreases CRC cell viability

In order to assess the synergism between doped and undoped NCs and SW, both cell lines were preincubated with 10 μg/ml of ZnO NCs or Fe:ZnO NCs for 24 h and then exposed to a single SW treatment (0.12 mJ/mm^2, 250 shots, 4 shots/s) assessing the cell viability after 24, 48 and 72 h and comparing to the untreated control, as well as to the NCs or SW only treated controls. As reported in Fig. 5A, the combination treatment with undoped/doped NCs + SW did not display an augmented mortality of HT-29 cells

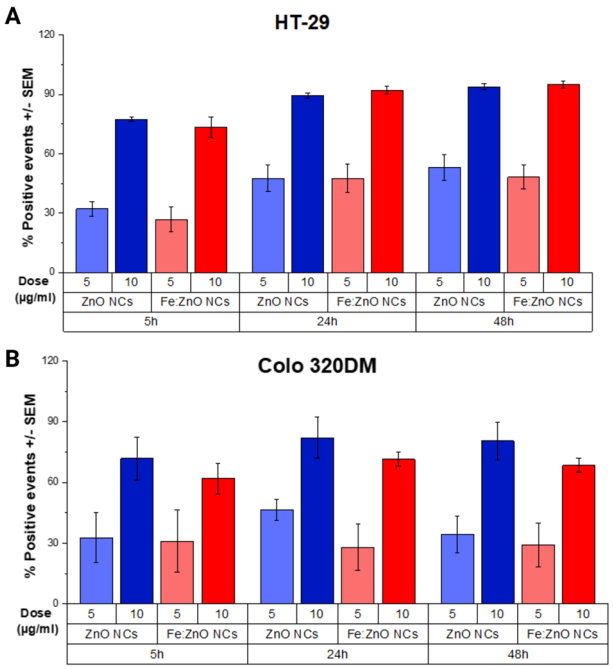

Fig. 4 ZnO NCs and Fe:ZnO NCs internalization in HT-29 (**A**l) and Colo 320DM (**B**) at two different concentrations (5 and 10 μg/ml) and different time points (5 h, 24 h, 48 h). Data are expressed as percentage of positive events mean ± SEM. n ≥ 3

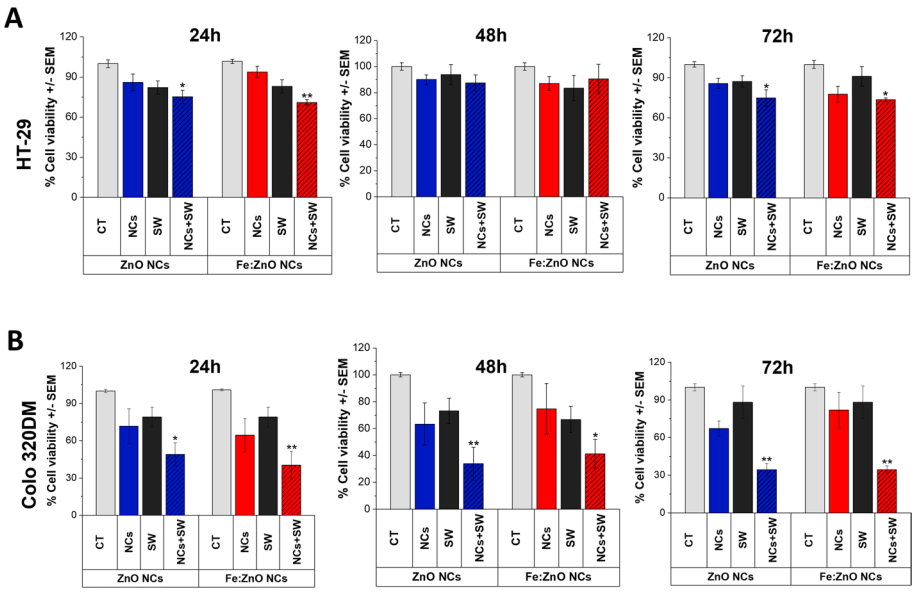

Fig. 5 The effects of ZnO NCs and Fe:ZnO NCs incubation and single SW treatment in **A** HT-29 and **B** Colo 320DM cells. Both cell lines were incubated with 10 µg/ml of NCs in 96-well plates in replicates. After 24 h of NCs incubation, cells were exposed to 250 shots of SW (0.12 mJ/mm.^{2}, 4 shots/s). Control experiments were also carried out for comparison. CT represents untreated control cells; NCs are cells exposed only to ZnO NCs or Fe:ZnO NC; SW represents cells exposed to SW; NCs + SW are cells subjected to the combined treatment. After 24, 48 and 72 h, the cell viability was recorder by the WST-1 assay. Data are expressed as mean of cell viability ± SEM. n ≥ 3. Statistical relevance is indicated in comparison with control sample (*$p < 0.05$, **$p < 0.01$, ***$p < 0.001$)

at all the considered time points (with a cell viability above 70%), even if some statistically relevant differences in comparison to control cells were reported at 24 h and 72 h. However, no statistically significant difference was observed in HT-29 cells between SW treatment and NCs + SW treatment neither with ZnO NCs nor with Fe:ZnO NCs (see the complete statistical analysis in Additional file 1). On the contrary, Colo 320DM cells treated with both NCs and SW (Fig. 5B) always showed a significant decrease of cell proliferation in comparison with control cells (CT) starting 24 h after the SW treatments. Remarkably, neither the SW treatment alone nor the NCs alone were able to trigger cell death, suggesting that only the combined approach exerts the desired mortality. This synergistic effect is further maximized 72 h after the SW exposure, when it is reported a significant decrease of cell viability between NCs + SW and SW, with a $p < 0.05$ for the comparisons between ZnO NCs + SW and SW, or Fe:ZnO NCs + SW and SW, as reported in the S.I., indicating that cells were not able to recover after the combined NCs + SW treatment.

Successively, based on our previous data obtained in a cervical adenocarcinoma model (Racca et al. 2020), where we highlighted the efficacy of three consecutive SW treatments after the NCs exposure, we decided to explore the same 3SW treatment against both CRC cell lines. As shown for singular SW exposure, the combined treatment with undoped/doped NCs + 3SW was highly effective against Colo 320DM cells (Fig. 6B), while it resulted less effective on HT-29 cells (Fig. 6A), even if some significant differences against CT were noticed even in this CRC cell line. Remarkably, Colo 320DM cells greatly suffered the combined treatment, with a high decrease of cell viability (mean:

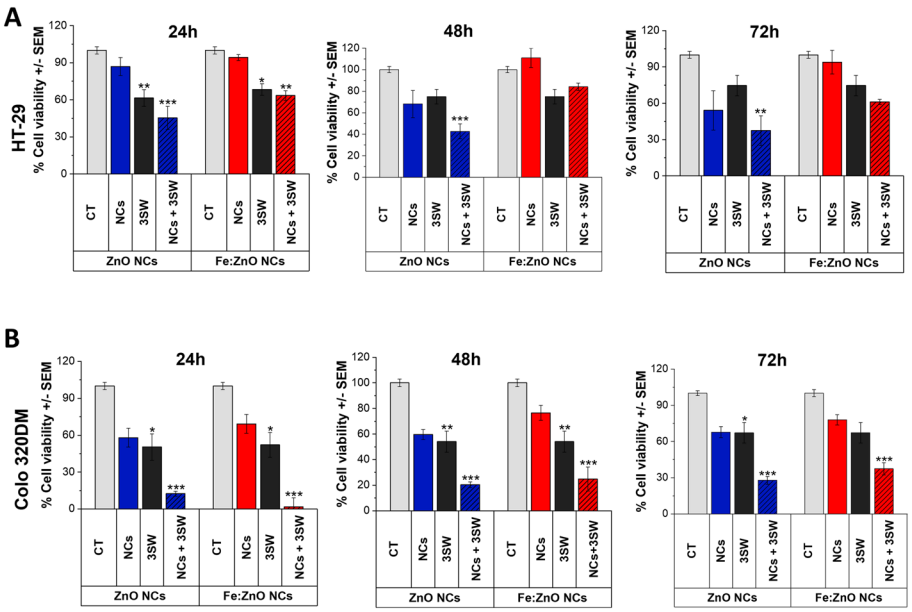

Fig. 6 The effects of ZnO NCs and Fe:ZnO NCs ZnO NCs incubation and 3SW treatments in **A** HT-29 and **B** Colo 320DM cells. Both cell lines were incubated with 10 µg/ml of NCs in 96-well plates in replicates. After 24 h of NCs incubation, wells were exposed to 250 shots of SW (0.12 mJ/mm.^{2} 4 shots/s) for three times (a treatment every 4 h), while control cells remained untreated or received only the NCs or 3SW treatments. CT represents untreated cells; NCs are cells exposed only to ZnO NCs or Fe:ZnO NC; 3SW represents cells exposed to SW for three times; NCs + 3SW are cells subjected to the combined treatment. After 24, 48 and 72 h, the cell viability was recorder by the WST-1 assay. Data are expressed as mean on cell viability with relative to untreated cells ± SEM. n ≥ 3. Statistical relevance is indicated in comparison with control sample (*p < 0.05, **p < 0.01, ***p < 0.001)

12 ± 2% with ZnO NCs + 3SW, 2 ± 7% with Fe:ZnO NCs + 3SW) at 24 h, very far from the 50 ± 10% obtained by the control cells treated with only 3SW. The difference between cells exposed to NCs + 3SW and cells exposed to 3SW or NCs only is still maintained at 48 h and 72 h. The complete statistical analysis is reported in the S.I.

NC and shockwaves combined treatment compromises cell membrane integrity

The PI assay was employed to assess the membrane integrity after the combined treatment between ZnO NCs or Fe:ZnO NCs and 3SW. Cells were examined immediately after each single SW treatment, in order to observe the immediate effects on cells, and after 24, 48 and 72 h from the last 3SW treatment to evaluate the impact on cell membrane integrity. Data were acquired for both cell lines and with either ZnO NCs or Fe:ZnO NCs and fully reported in Additional file 1: Figures S3–S6. A representative trend is reported in Fig. 7, showing HT-29 (panel A) and Colo 320DM cells (panel B) incubated with Fe:ZnO NCs, 24 h after the last 3SW treatment. The images with a 20 × objective display a large field of view, in order to spot the average trend of the cell culture in the different conditions. It is worth noting that both the control samples and the NCs-treated cells show a negligible PI signal, suggesting that the cell membranes are preserved. On the contrary, the cells treated with 3SW (both with and without NCs) present a strong red fluorescent signal, indicating that the mechanical waves can damage the cell membrane. Furthermore, in the combined treatment of NCs and 3SW, the

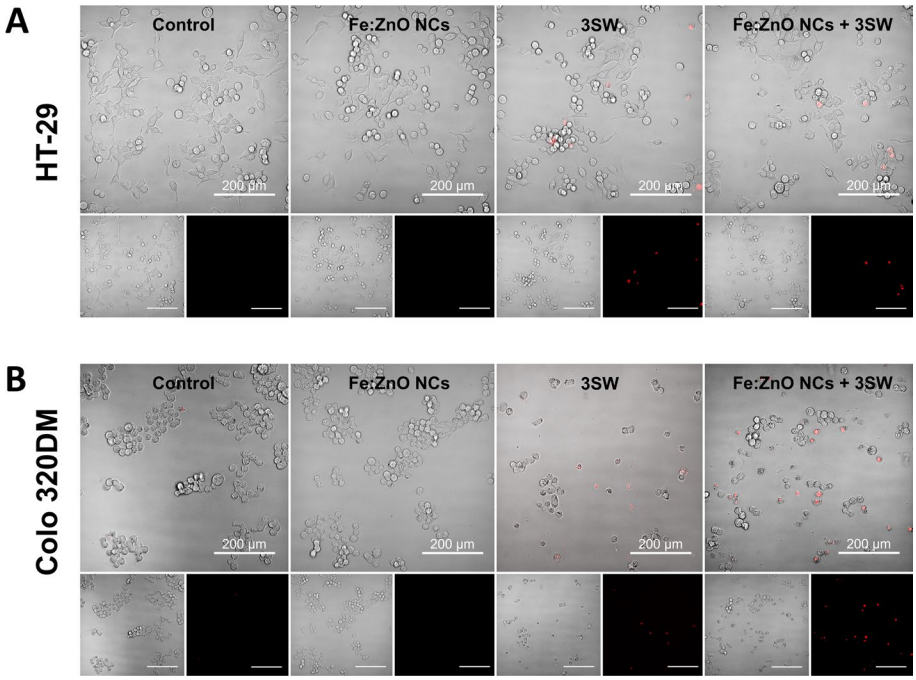

Fig. 7 Cell membrane integrity assay 24 h after the third SW treatment in **A** HT-29 and **B** Colo 320DM cells incubated with 10 µg/ml of Fe:ZnO NCs in 96-well plates. After 24 h of NCs incubation, cells were exposed to 250 shots of SW (0.12 mJ/mm^2, 4 shots/s) for three times (a treatment every 4 h), while control cells were not exposed, or were treated with Fe:ZnO NCs or 3SW only. 24 h after the third treatment, the cell culture medium was replaced with 1.5 µM propidium iodine (as indicator of membrane integrity) in PBS phosphate saline buffer. Cells were then observed under a wide-field fluorescence-inverted microscope (Eclipse Ti-E, Nikon) with 20X magnification objective lens. Scale bar is 200 µm

PI fluorescence is significantly enhanced, compared to the one of the 3SW alone, corroborating the hypothesis of the synergistic effect, also confirming the cytotoxicity data of Fig. 6. This synergy is more evident in Colo 320DM cell lines: interestingly, the PI fluorescence is higher immediately after the second SW treatment (Additional file 1: Figures S4 and S6), where the cells are damaged, but still adherent to the well plate. From the third SW treatment, cell death significantly starts to increase: cells get detached from the well plate and are thus eliminated during the substitution of the culture media with the PI solution. This corresponds in the images to a drastically lower number of cells in samples treated with 3SW. Remarkably, the membrane damage persists over time, as an abundant PI fluorescence is visible (especially in the samples with combined NCs and 3SW treatment) also in the 24, 48 and even 72 h time steps.

In contrast, the evaluation about the production of reactive oxygen species from the ZnO and Fe:ZnO NCs in water media and activated by SW was not proven (Additional file 1: Figure S7). Therefore, cell death mechanism caused by ROS production is here ruled out.

Combined treatment prevalently induces apoptotic cell death in CRC cells

Since the highest mortality was obtained on Colo 320 DM after the treatment with NCs and SW, even after one SW treatment, further analyses on the kinetic of cell death were performed on this cell line only. The cell responses were thus monitored after

co-incubation with NCs (doped and undoped) and after a single SW exposure, measuring the obtained signals at different time points up to 24 h after the treatment. The luminescent signal, due to the exposure of phosphatidylserine, characteristic of an early apoptotic pathway, augmented immediately after the SW exposure (0 min in Fig. 8A), and continued to increase up to 6 h after the treatment. The fluorescence signal, due to the fluorescent intercalating DNA probe as indicator of late apoptosis and necrosis, increases slowly from the beginning up to 24 h. A modest increase was already measured at 0 min, immediately after treatment with SW (with or without NCs), but remained constant up to 6 h, and started to increase only 24 h later (Fig. 8B). The trends of the two signals together suggest the prevalence of an apoptotic pathway, characterized by a first marked increase in luminescence, followed by an increase in fluorescence, even if some events of necrosis, suggested by the slight rise of the fluorescence signal immediately after the SW treatment, could not be excluded. Remarkably, the CRC cells treated with both NCs and SW always showed higher luminescence and fluorescence signals than the ones treated with NCs or SW separately, in accordance with the WST-1 data.

Discussion

The present work aims to validate ZnO and Fe:ZnO NCs as therapeutic agents in synergy with SW against CRC. This investigation was carried out on two different CRC cell lines with different features and behavior (HT-29 and Colo 320DM cells) in vitro.

From the physical and chemical points of view, ZnO NCs were synthesized by a wet chemistry approach with an oleic acid capping and a chemical functionalization with amino-propyl groups. These organic moieties at the nanoparticle surface confer a high colloidal stability to the NCs and the presence of amine groups help to increase the Z-potential values and to covalently bind fluorescent dyes, useful for cytofluorimetric investigations. The NCs were also doped with iron, which was already shown to improve the zinc oxide stability against fast dissolution into zinc cations (Zn^{2+}) and increase its biocompatibility towards cells (Carofiglio et al. 2020; Xia et al. 2011; Manshian et al. 2017). Furthermore, iron-doped zinc oxide nanocrystals were also reported to have

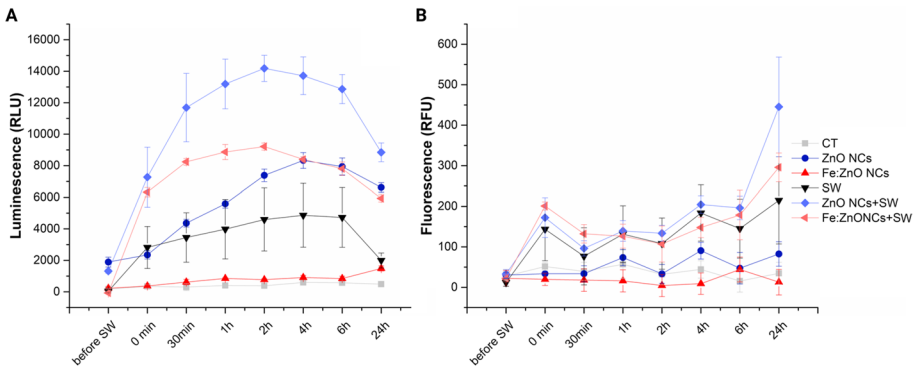

Fig. 8 Kinetic of cell death in the NCs + SW experiment in Colo 320DM cells. Luminescence (**A)** is expressed as relative light units (RLU), and fluorescence (**B)** is expressed as relative fluorescence units (RFU), measurements. Colo 320DM cells were considered alone (CT), treated with 10 µg/ml NCs for 24 h (ZnO NCs or Fe:ZnO NCs), treated with SW alone (SW), or incubated with NCs and then treated with SW (ZnO NCs + SW and Fe:ZnO NCs + SW). The two signals were recorded before SW exposure (before SW), immediately after SW administration (0 min), and several time points after the SW treatment (30 min, 1 h, 2 h, 4 h, 6 h and 24 h)

magnetic properties, which are not shown in the undoped counterpart (Carofiglio et al. 2021). Actually, the magnetic properties allow a very attractive perspective for future in vivo application, such as a nano-contrast agent for magnetic resonance imaging.

In this work, the biological investigation started comparing the cytotoxicity and the internalization rate of doped and undoped NCs on CRC cell lines. ZnO NCs are generally extremely toxic for cancer cells when reduced to nanosized dimension, as already reported (Racca et al. 2018). In the present study, we confirmed this behavior, but we also highlighted that iron-doped ZnO NCs were less toxic than their undoped counterpart especially to HT-29 cells, while showing almost the same toxicity trend in Colo 320DM cells. Since the same protocol was employed for both cell lines, thus limiting the variability due to different experimental settings (Canta and Cauda 2020), it is reasonable to suppose a different susceptibility of these cell lines to ZnO NCs and Fe:ZnO NCs. The reduced Zn^{2+} cation release from Fe:ZnO NCs, proved in the previous literature reports (Carofiglio et al. 2020; Xia et al. 2011), is anyway sufficient to affect the viability of Colo 320DM cells, being this cell line probably influenced by the zinc cation imbalance as well as by other ZnO toxicity mechanisms, e.g., ROS production (Racca et al. 2018).

Several experiments were carried out to find a possible synergism between one or multiple SW treatments with undoped and doped NCs in CRC cell lines, trying to trigger a cytotoxic effect. We previously proved that three consecutive treatments were necessary to achieve cervical adenocarcinoma cancer cell death (Racca et al. 2020). In the present case, HT-29 cells do not show any serious consequence to the combined action of NCs + SW with one single SW treatment, while a more marked decrease of cell viability was observed after 3SW treatments, confirming our previous results. Remarkably, Colo 320DM cells viability was significantly affected even after the NCs + SW single administration and was further maximized after 3SW administration. The obtained results were similar either using ZnO NCs or Fe:ZnO NCs. We can therefore state that the effect of SW treatment firstly depends on the features of each kind of tumor cells.

As mentioned above, the mechanism of interaction between nanoparticles and mechanical pressure waves has not been entirely understood yet. Actually, it is reported that the addition of nanoparticles decreases the cavitation threshold, i.e., the power density of pressure waves necessary to obtain the acoustic cavitation. This is a phenomenon related to the generation and implosion of microbubbles originating from the gas pockets already present in the treated solution or in the body (Ancona et al. 2020). The cyclic oscillation and implosion of these bubbles, due to the acoustic pressure, cause temperature increase, mechanical stress and reactive oxygen species production, thus stressing cancer cells (Canavese et al. 2018; Izadifar et al. 2017; Sviridov et al. 2015). In addition, bubbles collapse results in light emission that could activate ZnO nanoparticles to produce ROS, as in the case of photodynamic therapy (Vighetto et al. 2022). Furthermore, the simple nanoparticles oscillation under the mechanical wave stimulation could mechanically perturb the cells, a phenomenon described as "nanoscalpel" (Osminkina et al. 2015) or "nanodrill" effect (Vighetto et al. 2021) depending on where the nanoparticles are located inside the cells. In addition, when considering ZnO nanomaterials, their degradation in biological media can produce the release of toxic Zn^{2+} cations, that could poison the cells (Seil and Webster 2012). Finally, another mechanism could be hypothesized, since the mechanical stimulation of a piezoelectric material such as ZnO and even

more iron-doped ZnO could result in the generation of electric charge, that could imbalance cell functionality (Marino et al. 2018; Marino et al. 2019; Carofiglio et al. 2021). This last aspect was not directly observed here and in the present work remains a further hypothesis to be explored.

Furthermore, it was already demonstrated that ROS are not truly responsible for cell death in the case of NCs activated by SW (Racca et al. 2020), therefore other mechanisms, like mechanical injury of cells can be considered. In the present paper, we specifically ruled out the generation of ROS, as these species were not detected by the SW activated NCs in water, neither by the NCs alone. A possible explanation for this phenomenon might be that the excitation frequency of SW is not suitable to establish any cavitation phenomena. An alternative explanation can also be that the DMPO trap is not sensitive to the specific radicals formed in response to this stimulation. Therefore, ROS generation, if potentially present, may not be provoked by the combination of SW and NPs, and thus it is excluded from being the main responsible for the observed cell death.

Concerning the PI assay, it highlighted an increased number of red cells, i.e., cell with a perturbed membrane, particularly when both NCs and SW were present. This mechanism can be probably due to a combination of the mechanical stress provoked by the cavitating bubble (under oscillation and or implosion) and the motion of NCs under the SW exposure. It could not be excluded that membrane perturbation and thus PI fluorescence could be also related to necrosis mechanisms.

As highlighted above, several hypotheses could be thus formulated to explain why the synergy between NCs and SW worked in efficiently killing the Colo 320DM cells. In contrast, the same mechanisms were less efficient in HT-29 cells and some considerations should be made. First of all, the two cell lines have different origins, i.e., Colo 320DM are a Duke's type C carcinoma and possess different features compared to HT-29 cells: their shape is quite rounder than the HT-29, they are weakly attached to the bottom of the plate, and they do not form dense cell colonies (Tommelein et al. 2016). Moreover, HT-29 cells have an epithelial phenotype compared to the more mesenchymal one of Colo 320DM cells, as evidenced by the absence of the Epithelial Splicing regulatory protein 1 (ESRP1) expression (Fagoonee et al. 2017). It was indeed shown that mesenchymal cells are more susceptible to shock waves (Foglietta et al. 2017). Furthermore, it was already reported that the susceptibility to mechanical pressure wave stimulation is influenced by geometrical factor, such as shape: this factor could possibly explain why a rounder cancer cell line as Colo 320DM can be generally more damaged by mechanical waves than the HT-29 one (Trendowski 2014).

Furthermore, observing the cytotoxicity results, HT-29 were very less sensitive to NCs and especially to the iron-doped ones (Fe:ZnO NCs). In contrast, Colo 320DM cells were more susceptible to doped and undoped NCs, even if the cell viability was never below 60% up to 10 μg/ml of NCs concentration. Probably this cell line underwent diverse toxicity mechanisms compared to HT-29. Indeed, it could be hypothesized that the cell's first response to NC's toxicity drives the further outcomes with SW: cells already affected by the administration of doped or undoped NCs are more harmed by the subsequent SW treatment. In this case, the "poisoning" of Colo 320DM cells by the further release of Zn^{2+} cations resulted in an increased susceptibility to SW treatment, opening the possibility to another possible motivation for the functioning of the synergy

NCs + SW. Indeed, when exploring the kinetic of cell death through a dedicated assay in Colo 320DM cells, that recorded the highest mortality even after a single SW treatment and a trend compatible with an apoptotic phenotype was reported immediately after the SW treatment up to 24 h. Noticeably, both luminescence and fluorescence signals were always increased by the combined action of doped or undoped NCs and SW, confirming the presence of a more marked cell sufferance. All togherther, the trends observed seem to suggest an apoptotic pathway, with an increased luminescence followed by an augmented fluorescence, confirming the previously collected data on adenocarcinoma cell lines (Racca et al. 2020).

Conclusions

In this work, we proposed a stimuli-responsive treatment based on the combination of zinc oxide nanocrystals and mechanical pressure waves, i.e., shock waves, against CRC cell lines. ZnO NCs were synthesized with an oleic acid capping and amino-propyl functionalization and a comparison with iron-doped and undoped ZnO nanoparticles was carried out from a physical–chemical point of view and in terms of cell interaction and therapeutic activity. Two CRC lines were tested, i.e., HT-29 and Colo 320DM, the first with an epithelial phenotype, while the second a mesenchymal one. An important cytotoxicity was triggered when combining either undoped or iron-doped ZnO NCs with shock waves especially on Colo 320DM cell line, while cells remained almost unaffected when the treatments were carried out separately. Single versus multiple stimulations were also proved to produce similar effects when combined to NCs administration. Various cytotoxicity mechanisms were hypothesized to unravel the toxicity of the combined treatment, i.e., NCs + SW, involving cell membrane destabilization and inducing a remarkable apoptosis events on Colo 320DM cell line. In contrast, the generation of ROS, specifically of hydroxyl radicals, was here ruled out. More work needs to be done in vivo to assess the biosafety, bio-distribution, and the potential antitumor effect of this system in the presence of vascularization, immune cells as well as the related biomechanical consequences. However, the obtained proof-of-concept results pave the way for a deeper study towards clinical translation. The advantages of the proposed synergistic activity rely on the use of potentially theranostic nanoparticles having magnetic properties and an on-demand therapeutic activity once activated by shock waves. In addition, SW allows the ease treatment of even deep-seated tumor masses, opening new perspectives in nanomedicine-based therapeutic approaches while monitoring the state of the disease. Further improvements can envision the use of nanoparticles with improved biomimicry and active targeting against the diseased tissue or its microenvironment, with the final aim to clinically translate the proposed synergistic approach.

Supporting information

The following files are available: Magnetic behavior of ZnO and Fe:ZnO NCs. Representative curves of fluorescent intensity measured by flow cytometer for the quantification of cellular uptake of Atto-647-NHS ester-labelled NCs in CRC cell lines. Cell membrane permeability examined with PI under wide-field optical fluorescence microscope 24 h after ZnO NC and Fe:ZnO NCs and SW, 24-48-72h after ZnO NCs and Fe:ZnO NCs

with 3SW, and after each SW treatment during the multiple 3SW. Statistical analysis for cytotoxicity, SW and 3SW treatments. ROS generation under SW stimulation.

Supplementary Information

The online version contains supplementary material available at https://doi.org/10.1186/s12645-023-00195-6.

Additional file 1: Figure S1. DC magnetization measurements of ZnO and Fe:ZnO NCs. The graph shows the magnetization of 1 mg of NCs embedded in Durcupan ACM resin (Sigma-Aldrich) measured by means of a DC magnetometer (Lake Shore 7225, Lake Shore Cryotronics) at room temperature and in quasistatic conditions. **Figure S2.** Fluorescent intensity measured by flow cytometer Guava Easycyte 6-2L (Merck Millipore) for the quantification of cellular uptake of Atto-647-NHS ester-labeled NCs in (A) HT-29 and (B) Colo 320DM cell lines. Measurements were performed 5, 24 and 48 h after treatment with fluorescently labeled ZnO NCs or Fe:ZnO NCs at a concentration of 0, (control) 5 or 10 μg/mL. **Figure S3.** Cell membrane integrity assay of **Fe:ZnO NCs**—co-incubated and 3SW-treated **HT-29**. Cells were observed under a wide-field fluorescence-inverted microscope (Eclipse Ti-E, Nikon) with 20X magnification objective lens, after each SW treatment and 24, 48, and 72 h after the last SW treatment. **Figure S4.**Cell membrane integrity assay of Fe:ZnO NCs—co-incubated and 3SW-treated Colo 320DM. Cells were observed under a wide-field fluorescence-inverted microscope (Eclipse Ti-E, Nikon) with 20X magnification objective lens, after each SW treatment and 24, 48, and 72 h after the last SW treatment. **Figure S5**. Cell membrane integrity assay of ZnO NCs—co-incubated and 3SW-treated HT-29. Cells were observed under a wide-field fluorescence-inverted microscope (Eclipse Ti-E, Nikon) after each SW treatment (20X magnification objective lens) and 24, 48, and 72 h after the last SW treatment (40X objective lens). **Figure S6**. Cell membrane integrity assay of ZnO NCs—co-incubated and 3SW-treated Colo 320DM. Cells were observed under a wide-field fluorescence-inverted microscope (Eclipse Ti-E, Nikon) after each SW treatment (20X magnification objective lens) and 24, 48, and 72 h after the last SW treatment (40X objective lens). **Figure S7**. Electron paramagnetic resonance (EPR) spectroscopy analysis of Fe:ZnO and ZnO NCs dispersed in water and stimulated with SW. The typical spin-adduct of DMPO-OH (an example is reported on the top of the graph) has been detected neither in pure water nor in presence of ZnO and Fe:ZnO NCs (15 μg/mL) after the SW stimulation.

Acknowledgements
The authors wish also to thank the company ELvation Medical GmbH for providing the instrument PiezoWave^2 from Richard Wolf.

Author contributions
LR and GR wrote the manuscript text; LR set Fig. 8; GR set Figs. 1, 3–7 and those in the S.I.; LR, GR, SF and GM set the methodology and carried the biological experiments; MC prepared and characterized the nanoparticles and set Fig. 2; FA supervised the biological methodology and experiments; VC conceived and supervised the whole work, acquired and managed funding and collaborations. All authors reviewed the manuscript and have given approval to the final version of the manuscript. All authors read and approved the final manuscript.

Funding
This work has received funding from the European Research Council (ERC) under the European Union's Horizon 2020 Research and Innovation Program (Grant agreement No. 678151—Project Acronym "TROJANANOHORSE"—ERC starting Grant and Grant agreement No. 957563—Project Acronym "957563— XtraUS"—ERC Proof of Concept Grant).

Availability of data and materials
All data generated or analyzed during this study are included in this published article and its supplementary information files.

Declarations

Ethics approval and consent to participate
Not applicable.

Consent for publication
Not applicable.

Competing interests
The authors declare that they have no competing interests.

Received: 12 October 2022 Accepted: 8 April 2023
Published online: 19 April 2023

References

Ancona A et al (2018) Lipid-coated zinc oxide nanoparticles as innovative ROS-generators for photodynamic therapy in cancer cells. Nanomaterials. https://doi.org/10.3390/nano8030143

Ancona A, Troia A, Garino N, Dumontel B, Cauda V, Canavese G (2020) Leveraging re-chargeable nanobubbles on amine-functionalized ZnO nanocrystals for sustained ultrasound cavitation towards echographic imaging. Ultrason Sonochem. https://doi.org/10.1016/j.ultsonch.2020.105132
Barui S, Gerbaldo R, Garino N, Brescia R, Laviano F, Cauda V (2020) Facile chemical synthesis of doped ZnO nanocrystals exploiting oleic acid. Nanomaterials 10(6):1–15. https://doi.org/10.3390/nano10061150
Beik J et al (2018) Gold nanoparticle-induced sonosensitization enhances the antitumor activity of ultrasound in colon tumor-bearing mice. Med Phys 45(9):4306–4314. https://doi.org/10.1002/mp.13100
Bharat TC, Shubham, Mondal S, Gupta HS, Singh PK, Das AK (2019) Synthesis of doped zinc oxide nanoparticles: a review. Mater Today Proc 11:767–775. https://doi.org/10.1016/j.matpr.2019.03.041
Brar B et al (2021) Nanotechnology in colorectal cancer for precision diagnosis and therapy. Front Nanotechnol. https://doi.org/10.3389/fnano.2021.699266
Cabeza L et al (2020) Nanoparticles in colorectal cancer therapy: latest in vivo assays, clinical trials, and patents. AAPS PharmSciTech 21(5):178. https://doi.org/10.1208/s12249-020-01731-y
Canavese G et al (2018) Nanoparticle-assisted ultrasound: a special focus on sonodynamic therapy against cancer. Chem Eng J 340:155–172. https://doi.org/10.1016/j.cej.2018.01.060
Canta M, Cauda V (2020) The investigation of the parameters affecting the ZnO nanoparticle cytotoxicity behaviour: a tutorial review. Biomater Sci 8(22):6157–6174. https://doi.org/10.1039/d0bm01086c
Carofiglio M, Barui S, Cauda V, Laurenti M (2020) Doped zinc oxide nanoparticles: synthesis, characterization and potential use in nanomedicine. Appl Sci. https://doi.org/10.3390/app10155194
Carofiglio M, Laurenti M, Genchi GG, Ciofani G, Grochowicz M, Cauda V (2021) Ultrasound triggered ZnO-based devices for tunable and multifaceted biomedical applications. Adv Mater Interfaces 8(21):2101021. https://doi.org/10.1002/admi.202101021
Carofiglio M et al (2021) "Iron-Doped ZnO nanoparticles as multifunctional nanoplatforms for theranostics. Nanomaterials. https://doi.org/10.3390/nano11102628
Cisterna BA, Kamaly N, Il Choi W, Tavakkoli A, Farokhzad OC, Vilos C (2016) Targeted nanoparticles for colorectal cancer. Nanomedicine (lond) 11(18):2443–2456. https://doi.org/10.2217/nnm-2016-0194
Dumontel B et al (2017) Enhanced biostability and cellular uptake of zinc oxide nanocrystals shielded with a phospholipid bilayer. J Mater Chem B 5(44):8799–8813. https://doi.org/10.1039/C7TB02229H
Dumontel B et al (2019) ZnO nanocrystals shuttled by extracellular vesicles as effective Trojan nano-horses against cancer cells. Nanomedicine (lond) 14(21):2815–2833. https://doi.org/10.2217/nnm-2019-0231
Fagoonee S et al (2017) The RNA-binding protein ESRP1 promotes human colorectal cancer progression. Oncotarget 8(6):10007–10024. https://doi.org/10.18632/oncotarget.14318
Foglietta F et al (2017) Selective sensitiveness of mesenchymal stem cells to shock waves leads to anticancer effect in human cancer cell co-cultures. Life Sci 173:28–35. https://doi.org/10.1016/j.lfs.2017.01.009
Fuentes-Vélez S et al (2021) Impedance-based drug-resistance characterization of colon cancer cells through real-time cell culture monitoring. Talanta 222:121441. https://doi.org/10.1016/j.talanta.2020.121441
Garino N et al (2019) A microwave-assisted synthesis of zinc oxide nanocrystals finely tuned for biological applications. Nanomaterials 9(2):212. https://doi.org/10.3390/nano9020212
Goodrich GP, Bao L, Gill-Sharp KL, Sang KL, Wang JC, Payne JD (2010) Photothermal therapy in a murine colon cancer model using near-infrared absorbing gold nanorods. J Biomed Opt 15(1):18001. https://doi.org/10.1117/1.3290817
Haq AI, Schneeweiss J, Kalsi V, Arya M (2009) The Dukes staging system: a cornerstone in the clinical management of colorectal cancer. Lancet Oncol. https://doi.org/10.1016/S1470-2045(09)70157-3
Izadifar Z, Babyn P, Chapman D (2017) Mechanical and biological effects of ultrasound: a review of present knowledge. Ultrasound Med Biol 43(6):1085–1104. https://doi.org/10.1016/j.ultrasmedbio.2017.01.023
Jiang J, Pi J, Cai J (2018) The advancing of zinc oxide nanoparticles for biomedical applications. Bioinorg Chem Appl 2018:1062562. https://doi.org/10.1155/2018/1062562
Laurenti M et al (2019) Graphene oxide finely tunes the bioactivity and drug delivery of mesoporous ZnO scaffolds. ACS Appl Mater Interfaces 11(1):449–456. https://doi.org/10.1021/acsami.8b20728
Liang S et al (2021) Conferring Ti-based MOFs with defects for enhanced sonodynamic cancer therapy. Adv Mater 33(18):2100333. https://doi.org/10.1002/adma.202100333
Liu J et al (2017) From the cover: ion-shedding zinc oxide nanoparticles induce microglial BV2 cell proliferation via the ERK and Akt signaling pathways. Toxicol Sci 156(1):167–178. https://doi.org/10.1093/toxsci/kfw241
Manco M et al (2021) The RNA-binding protein ESRP1 modulates the expression of RAC1b in colorectal cancer cells. Cancers. https://doi.org/10.3390/cancers13164092
Manshian BB et al (2017) In silico design of optimal dissolution kinetics of Fe-doped ZnO nanoparticles results in cancer-specific toxicity in a preclinical rodent model. Adv Healthc Mater 6(9):1601379. https://doi.org/10.1002/adhm.201601379
Marino A, Battaglini M, De Pasquale D, Degl'Innocenti A, Ciofani G (2018) Ultrasound-activated piezoelectric nanoparticles inhibit proliferation of breast cancer cells. Sci Rep 8(1):1–13. https://doi.org/10.1038/s41598-018-24697-1
Marino A et al (2019) Multifunctional temozolomide-loaded lipid superparamagnetic nanovectors: dual targeting and disintegration of glioblastoma spheroids by synergic chemotherapy and hyperthermia treatment. Nanoscale. https://doi.org/10.1039/c9nr07976a
Marino A et al (2019) Piezoelectric barium titanate nanostimulators for the treatment of glioblastoma multiforme. J Colloid Interface Sci 538:449–461. https://doi.org/10.1016/j.jcis.2018.12.014
Matos JC et al (2020) "Biomimetic amorphous Titania nanoparticles as ultrasound responding agents to improve cavitation and ROS production for sonodynamic therapy. Appl Sci. https://doi.org/10.3390/app10238479
Nompumelelo Simelane NW, Kruger CA, Abrahamse H (2020) Photodynamic diagnosis and photodynamic therapy of colorectal cancer in vitro and in vivo. RSC Adv 10(68):41560–41576. https://doi.org/10.1039/D0RA08617G
Osminkina LA et al (2015) Porous silicon nanoparticles as efficient sensitizers for sonodynamic therapy of cancer. Microporous Mesoporous Mater 210:169–175. https://doi.org/10.1016/j.micromeso.2015.02.037

Palzer J, Eckstein L, Slabu I, Reisen O, Neumann UP, Roeth AA (2021) Iron oxide nanoparticle-based hyperthermia as a treatment option in various gastrointestinal malignancies. Nanomaterials. https://doi.org/10.3390/nano11113013
Patterson AL (1939) The Scherrer formula for X-ray particle size determination. Phys Rev 56(10):978–982. https://doi.org/10.1103/PhysRev.56.978
Pavitra E et al (2021) Engineered nanoparticles for imaging and drug delivery in colorectal cancer. Semin Cancer Biol 69:293–306. https://doi.org/10.1016/j.semcancer.2019.06.017
Racca L, Cauda V (2021) Remotely activated nanoparticles for anticancer therapy. Nano-Micro Lett. https://doi.org/10.1007/s40820-020-00537-8
Racca L et al (2018) Zinc oxide nanostructures in biomedicine. Smart Nanoparticles Biomed. https://doi.org/10.1016/b978-0-12-814156-4.00012-4
Racca L et al (2020) Zinc oxide nanocrystals and high-energy shock waves: a new synergy for the treatment of cancer cells. Front Bioeng Biotechnol 8:577. https://doi.org/10.3389/fbioe.2020.00577
Sawicki T, Ruszkowska M, Danielewicz A, Niedźwiedzka E, Arłukowicz T, Przybyłowicz KE (2021) A review of colorectal cancer in terms of epidemiology, risk factors, development, symptoms and diagnosis. Cancers (basel) 13(9):2025. https://doi.org/10.3390/cancers13092025
Sazgarnia A et al (2013) Therapeutic effects of acoustic cavitation in the presence of gold nanoparticles on a colon tumor model. J Ultrasound Med 32(3):475–483. https://doi.org/10.7863/jum.2013.32.3.475
Seil JT, Webster TJ (2012) Antibacterial effect of zinc oxide nanoparticles combined with ultrasound. Nanotechnology 23(49):495101. https://doi.org/10.1088/0957-4484/23/49/495101
Skrajnowska D, Bobrowska-Korczak B (2019) Role of zinc in immune system and anti-cancer defense mechanisms. Nutrients 11(10):2273. https://doi.org/10.3390/nu11102273
Song Y, Guan R, Lyu F, Kang T, Wu Y, Chen X (2014) In vitro cytotoxicity of silver nanoparticles and zinc oxide nanoparticles to human epithelial colorectal adenocarcinoma (Caco-2) cells. Mutat Res Mol Mech Mutagen 769:113–118. https://doi.org/10.1016/j.mrfmmm.2014.08.001
Subramaniam VD, Ramachandran M, Marotta F, Banerjee A, Sun XF, Pathak S (2019) Comparative study on anti-proliferative potentials of zinc oxide and aluminium oxide nanoparticles in colon cancer cells. Acta Biomed 90(2):241–247. https://doi.org/10.23750/abm.v90i2.6939
Sung H et al (2021) Global cancer statistics 2020: GLOBOCAN estimates of incidence and mortality worldwide for 36 cancers in 185 Countries. CA Cancer J Clin 71(3):209–249. https://doi.org/10.3322/caac.21660
Sviridov AP, Osminkina LA, Nikolaev AL, Kudryavtsev AA, Vasiliev AN, Timoshenko VY (2015) Lowering of the cavitation threshold in aqueous suspensions of porous silicon nanoparticles for sonodynamic therapy applications. Appl Phys Lett. https://doi.org/10.1063/1.4931728
Tommelein J et al (2016) Age and cellular context influence rectal prolapse formation in mice with caecal wall colorectal cancer xenografts. Oncotarget 7(46):75603–75615. https://doi.org/10.18632/oncotarget.12312
Trendowski M (2014) The promise of sonodynamic therapy. Cancer Metastasis Rev. https://doi.org/10.1007/s10555-013-9461-5
Vighetto V et al (2019) The synergistic effect of nanocrystals combined with ultrasound in the generation of reactive oxygen species for biomedical applications. Front Bioeng Biotechnol 7(November):1–10. https://doi.org/10.3389/fbioe.2019.00374
Vighetto V et al (2021) Smart shockwave responsive Titania-based nanoparticles for cancer treatment. Pharmaceutics. https://doi.org/10.3390/pharmaceutics13091423
Vighetto V et al (2022) Insight into Sonoluminescence augmented by ZnO-functionalized nanoparticles. ACS Omega 7(8):6591–6600. https://doi.org/10.1021/acsomega.1c05837
Wan GY, Liu Y, Chen BW, Liu YY, Wang YS, Zhang N (2016) Recent advances of sonodynamic therapy in cancer treatment. Cancer Biol Med 13(3):325–338. https://doi.org/10.20892/j.issn.2095-3941.2016.0068
Xia T et al (2011) Decreased dissolution of ZnO by iron doping yields nanoparticles with reduced toxicity in the rodent lung and zebrafish embryos. ACS Nano 5(2):1223–1235. https://doi.org/10.1021/nn1028482
Xie Y-H, Chen Y-X, Fang J-Y (2020) Comprehensive review of targeted therapy for colorectal cancer. Signal Transduct Target Ther 5(1):22. https://doi.org/10.1038/s41392-020-0116-z
Zhang A-P, Sun Y-P (2004) Photocatalytic killing effect of TiO2 nanoparticles on Ls-174-t human colon carcinoma cells. World J Gastroenterol 10(21):3191–3193. https://doi.org/10.3748/wjg.v10.i21.3191
Zhong L, Yang T, Li P, Shi L, Lai J, Gu L (2022) Metal-organic framework-based nanotherapeutics with tumor hypoxia-relieving ability for synergistic sonodynamic/chemo-therapy. Front Mater. https://doi.org/10.3389/fmats.2022.841503

Publisher's Note